UCRL-JC-129752
PREPRINT

National Ignition Facility Main Laser Stray Light Analysis and Control

J. L. Miller
R. E. English
J. Schweyen
G. Peterson

This paper was prepared for submittal to the
Third Annual International Conference on Solid State Lasers for Application (SSLA) to Inertial Confinement Fusion (ICF)
Monterey, California
June 7-12, 1998

June 26, 1998

Lawrence Livermore National Laboratory

National Ignition Facility main laser stray light analysis and control

John L. Miller, R. Edward English

Lawrence Livermore National Laboratory, MS L-527, PO Box 808, Livermore, CA 94550

John Schweyen, Gary Peterson

Breault Research Organization,

ABSTRACT

Stray light analysis has been carried out for the main laser section of the National Ignition Facility main laser section using a comprehensive non-sequential ray trace model supplemented with additional ray trace and diffraction propagation modeling. This paper describes the analysis and control methodology, gives examples of ghost paths and required tilted lenses, baffles, absorbers, and beam dumps, and discusses analysis of stray light "pencil beams" in the system.

Keywords: ghost analysis, stray light, Nd:glass lasers, National Ignition Facility

1. INTRODUCTION AND METHODOLOGY

The National Ignition Facility is a target irradiation facility for research in Inertial Confinement Fusion. Each of the 192 main laser[1] beamlines is capable of producing an output energy of approximately 20kJ in a 3ns pulse at 1053nm. Figure 1 is a schematic drawing of the main laser optical system. The overall system is approximately 123m long, with optical apertures approximately 400mm square. The main laser beam lines include 16 nominally-transmitting surfaces that can act as sources of ghost reflections. These systems are 4-pass regenerative amplifiers, thus light travels through the components in two directions. In addition, stray light passes must be intercepted at the pinhole planes.

Figure 1

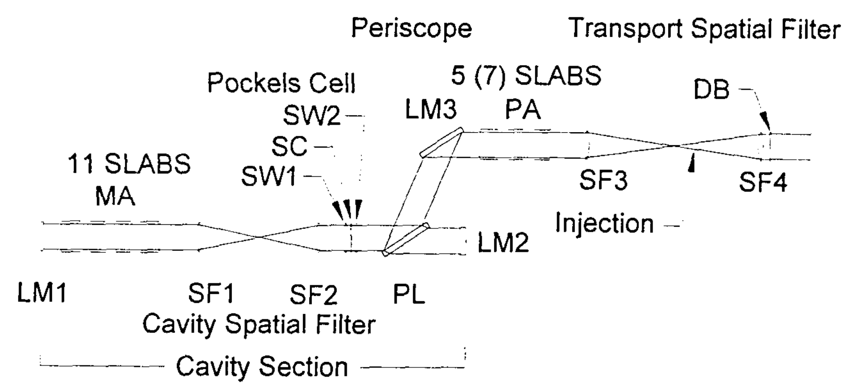

Our main tool for stray light analysis is a comprehensive non-sequential ray trace model for the full laser system. This is implemented using ASAP, and is used to calculate stray light fluences on all surfaces. In addition we carry out sequential surface ray trace calculations for backup, to aid with baffle design, and to use for tolerance studies. Diffraction analysis is performed for ghost foci that are potentially near surfaces. The diffraction propagation calculations are done using ASAP, or by calculating OPDs from OSLO and propagating using GLAD.

For the main laser layout, ghost stay-out zones are set using the criterion that fluences at surfaces due to ghosts must be less than 10% of the incident beam fluence. We specify non-metallic absorbers for all surfaces near optical elements which are irradiated with stray light fluences greater than the damage threshold of metals (typically assumed to be 100 mJ/cm^2). Absorber materials and locations are chosen such that the fluences at the absorbers are less than the damage threshold for the material. High fluence, cavity-type beam dumps are used for stray light passes near spatial filter pinhole planes. Metallic baffles are used to limit low-angle beam tube reflections where needed to block rays before foci. For this analysis, nominally-transmitting surfaces typically are modeled as having 1% reflectivity.

The non-sequential ray trace model for the main laser includes all optical surfaces, plus the pinhole geometry and mirror tilts needed to direct the beam along the 4-pass path. Multipass ray traces and OPD calculations for beams agree with results from other codes. Amplifier gain saturation is modeled by varying the gain through the multipass. The gains are varied to simulate different levels of saturation that result from varying output pulse energies. Last-photon gain values are used where appropriate for ghost paths. The 4-pass output energies agree with the laser physics models. The non-sequential ray trace model starts with the nominal input beam (from the injection system). As the beam propagates through the system the rays are "split" at ghost generating surfaces. These rays are tracked through the system, in turn splitting to higher order. The main advantage of this tool over sequential ray trace methods is that the accuracy of the results do not depend on anticipating significant ghost paths. Rather they are found implicitly. Mechanical features, such as lens bezels, beam tubes, spatial filter vessels, and optics mounts are represented in the model with sufficient resolution to calculate fluences at these surfaces accurately. Fluences at mechanical or optical surfaces usually are calculated using accumulated geometric ray densities. However, coherent (diffraction) propagation is used to evaluate fluences for significant ghost paths which have foci near surfaces. The coherent modeling technique used in ASAP involves Gaussian beam decomposition.

2. MAIN LASER GHOST EXAMPLES

This paper is not intended to list the ghosts and control measures comprehensively. Rather several examples will be given which illustrate typical, interesting, and difficult areas. The first example is the region that includes the main amplifier, that is between LM1 and SF1. This area is shown in figure 2, which also shows the diverging and converging ghost reflections from the lens for an incident pass 4 beam (incident from the left in fig. 2). The first order ghost focus

Figure 2

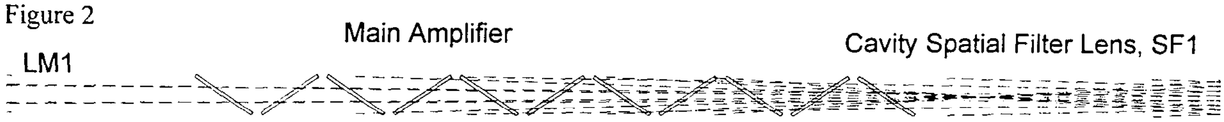

is 2765mm from the lens; this gives a stay-out zone that projects 3400mm from the lens. There several higher order ghost foci that are located farther from the lens that the first order ghost foci. However the higher order ghost foci all lie within the ghost stay-out zone. The 2 pass saturated gain in the main amplifier is about 17. Thus the reflected ghost light is amplified significantly. The calculated stray light fluence around the outside of LM1 is ~100 mJ/cm^2, the fluence around SF1 is ~200 mJ/cm^2. These are both locations where there is a marginal need for a non-metallic absorber to avoid having ablation products coat the optics. Another result of the gain is that the ghost light that returns to and through SF1 via a reflection off of LM1 is greatly enhanced: if all of the light from the pass 4-SF1 back reflections were contained by the beam tubes there would be ~4kJ in the amplified ghost beams; much of this energy would be deposited near the spatial filter pinholes. The amplified ghost energy is reduced by putting baffles in the beam tube to block low angle reflections, particularly in the space between the main amplifier and SF1.

The next example is the region between the cavity spatial filter pinhole plane and SF2. Figure 3 shows the cavity spatial filter structure for 24 beams (this is a vacuum spatial filter). The lenses are separated by about 23.5m. The structure comprises end vessels (with the lenses), beam tubes, and a central vessel. The pinhole plane includes a beam dump for pass 5. This is for light that remains in the cavity after the Pockels cell switches; the nominal pass 5 energy is 100 J. Excluding pass 5, a total of approximately 1 kJ of stray light is directed back toward the central vessel from or through SF2 surfaces. A consequence of the beam tube geometry is that some of the diverging ghost

Figure 3

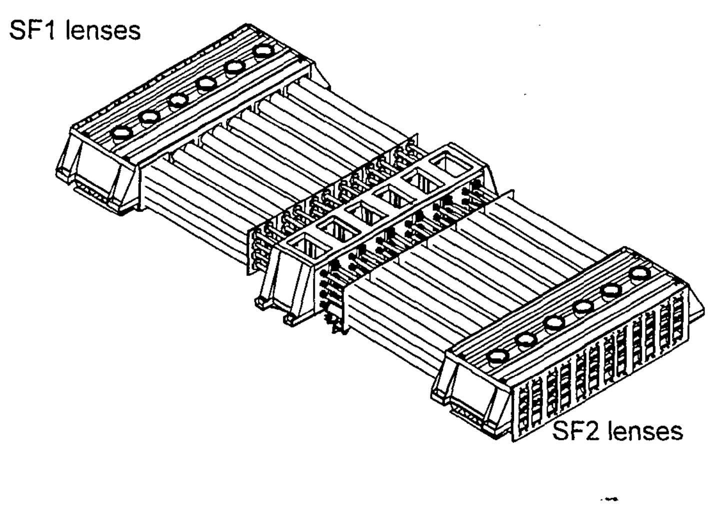

light from SF2 is concentrated by beam tube reflections at the pinhole plane. This is illustrated by figure 4. Approximately 20J is incident at the pinhole plane in a few square centimeters. The most significant ghost beams that enter this region come from Pockels cell reflections. The Pockels cell optics are wedged and tilted to deflect ghost reflections, the angles are shown in figure 5. The upper view in the figure is a top view of the assembly. The cell is rotated around the vertical axis to deflect the first order ghosts. A non-metallic absorber is placed in the cavity spatial filter beam tube, near the step between the small and large diameter circular tubes. The six first order ghosts have a total energy of ~800 J. The lower view in figure 5 is a side view. The elements are wedged and tilted around the horizontal axis to deflect second order ghosts. The angles shown in figure 5 are in units of mrad.

Figure 4: Concentration of ghost reflection light at cavity spatial filter pinhole plane by beam tube reflections

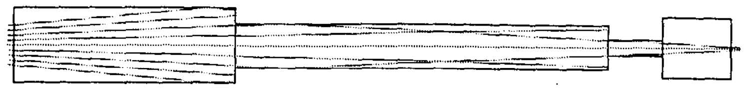

Figure 5

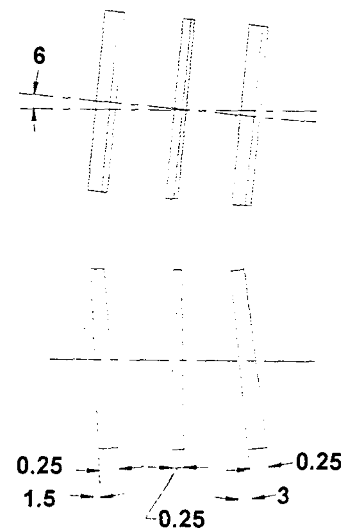

The region of the main laser where stray light control is most complex is between SF2 and LM2. Here there are 9 reflecting surfaces that participate in ghost reflections. There are a large number of ghost foci that are farther from SF2 than the first order foci. In particular there are 134 ghost foci from second through fourth order that are within 200mm of Pockels cell surfaces. A particularly troublesome ghost path leads to the second order ghost focus that is farthest from SF2. This is shown in figure 6. Pass 3 light is reflected from the inner surface of SF2, reflects off of LM2, then reflects again off of the inner surface of SF2. A 66mm diameter beam sub-aperture participates. The analysis of this ghost path includes OPD due to the pressure-induced deflection of SF2. The best focus is 3.3m from SF2. The wavefront error at focus is ~2 waves RMS. Using an random error of 0.25 waves in the incident beam, the resulting ghost peak fluence is 60 J/cm^2. This ghost is included in the stay-out zone away from SF2 (the Pockels cell is 3445mm from SF2). However, there are several third and fourth order ghosts that focus very close to Pockels cell or polarizer surfaces with focus fluences from 0.5 to 3 J/cm^2. These are essentially impossible to avoid.

Figure 6

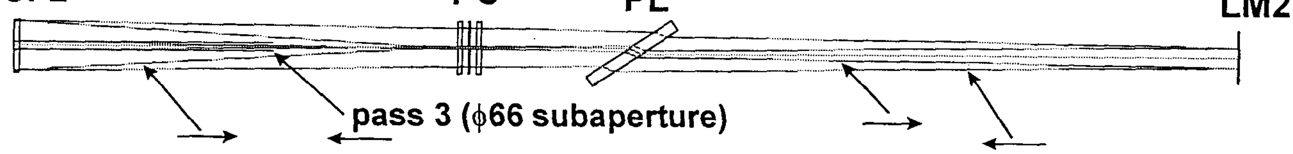

The next example is the region between LM3 and SF3 (this includes the power amplifier). The focal length of the transport spatial filter lenses is very long: 30m. Thus the first order ghost focus 7m from SF3. In order to decrease the stay out zone, SF3 is tilted by 2.8°. This is illustrated in figure 7, which is a top view of the area between the end of the power amplifier and SF3 for 2 adjacent beam columns. The rays shown coming from the top lens are the converging ghost, those from the bottom are the diverging ghost. The ghost beams are blocked by absorbing baffles on the wall of the beam tube between the beams. SF4 is also tilted, to

Figure 7

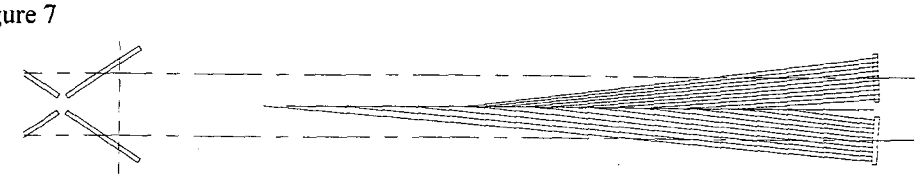

make these lenses identical. This deflects the SF4 ghosts into absorbers in the transport spatial filter end vessel.

The last example is between SF3 and the transport spatial filter pinhole plane. A high energy beam dump is needed at the pass 2 and 3 positions at the pinhole plane. The nominal pass 2 energy here is 120 J, due to Pockels cell/polarizer leakage. The need for a pass 3 dump here is more complicated: Light at the fundamental wavelength (1053nm) that is reflected from the target chamber along the output beam pass can travel backwards through the pass 4 pinholes in the transport and cavity spatial filters. After reflecting off of LM1 this beam will continue backwards along pass 3. The Pockels cell will be turned off, so the beam will reflect off of the polarizer and travel to the transport spatial filter. This beam could experience considerable gain by double-passing both the power and main amplifiers. It has been calculated that a 0.1% reflection at the target from a 5kJ shot would deposit 2.5kJ in the transport spatial filter pass 3 beam dump. Another source of stray light here is pass 4 second order Pockels cell ghosts. There are 15 such ghosts, each with a nominal energy of 2J. Three of the ghosts have very low angles with respect to pass 4: ~725μrad (the pinhole spacing is 1166μrad.) These 3 ghosts are due to reflections within the 3 Pockels cell optics. It isn't practical to block these beams much before focus. Thus they hit the pinhole baffle, 150mm in front of the pinhole plane. The estimated peak fluence is 600J/cm^2, but the predicted metal removal is just 0.5μm per shot.

3. PENCIL BEAMS

The ghost beams that have been discussed so far are isolated within sections of the laser due to the pinhole plane baffles. "Pencil beams", however, are able to propagate through the system, for up to several passes. The origin of pencil beams is shown in figure 8. Light from one of the beam paths exiting the cavity spatial filter reflects off of a lens surface and expands as it travels back toward the pinhole plane. Here some of the light is accepted by each of the 4 pinholes. Since this light went through a pinhole it can travel through the system and go through another pinhole.

Figure 8

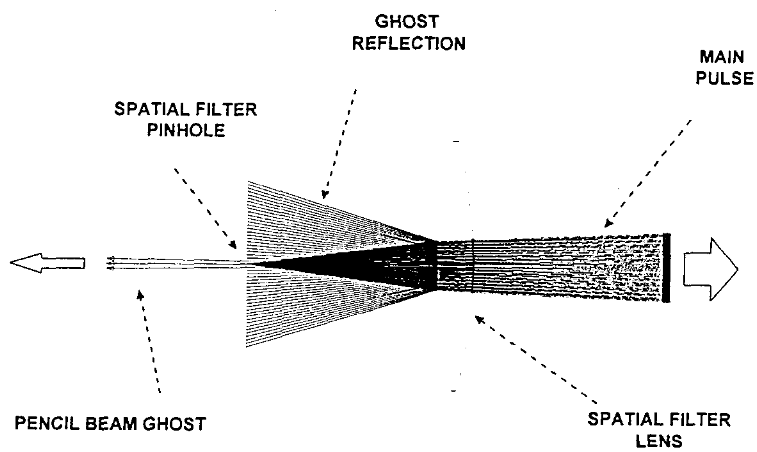

Pencil beams in the main laser have been analyzed extensively. During each pass, the main laser pulse spawns 2 ghosts at each lens; these, in turn, each generate 4 pencil beams. Pencil beams were evaluated at a series of pulse energies to characterize effects due to gain saturation varying with energy. It turns out that the pencil beam energy is maximum at an intermediate output energy. This happens because as the beam energy is reduced the initial pencil beam energy goes down. However the saturated gain in the amplifiers increases. The propagation of pencil beams was evaluated using wave optics. This accurately computes diffractive effects for beams with a low Fresnel number. This also facilitates the multipass propagation. Pencil beam timing with respect to the main pulse is tracked to model the effect of Pockels cell switching. The pencil beam fluence was evaluated at all optical surfaces, coherently summing the overlapping beams. Since the transport spatial filter lenses, SF3 and 4, are tilted, they do not generate pencil beams.

Figure 9

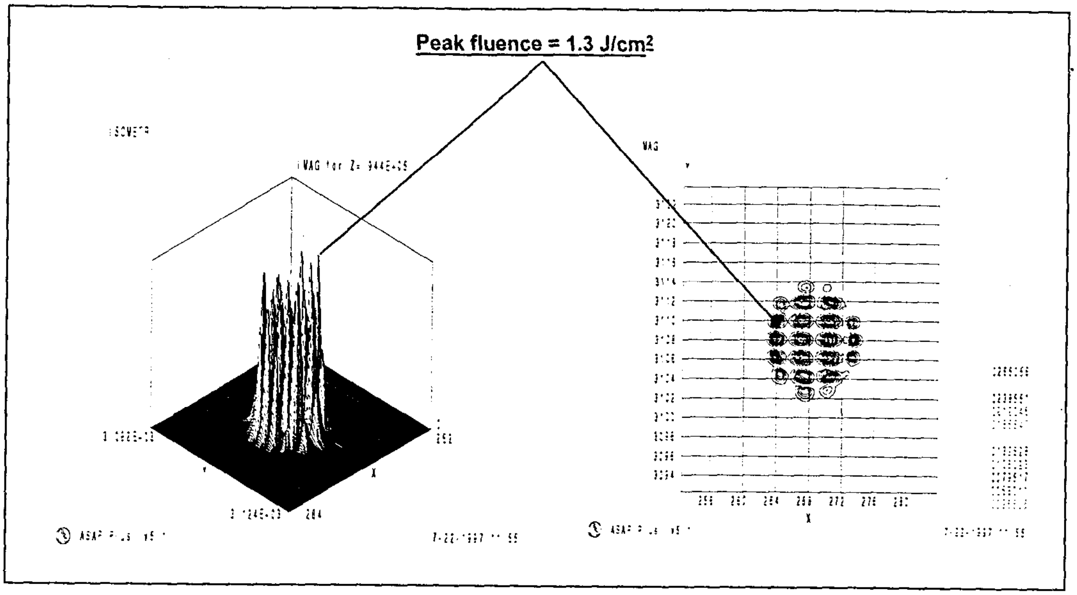

Much of the concern about pencil beams has centered on the injection mirror. Since this is very close to the transport spatial filter pinhole plane (1480mm), 4 pencil beams overlap. The calculated fluence distribution at the injection mirror is shown in figure 9. The peak coherent sum is 1.3J/cm^2 for a 7kJ output pulse.

Outside the spatial filter vessels the pencil beams come to very low Fresnel number foci. The highest calculated fluence near an optic due to pencil beams occurs near some of the first transport mirrors (LM4). Fortunately these are far enough away from the transport spatial filter that the pencil beams do not overlap. The resulting peak fluence is 2.8J/cm^2, also for a 7kJ output pulse. The calculated fluence distribution is shown in figure 10.

Figure 10

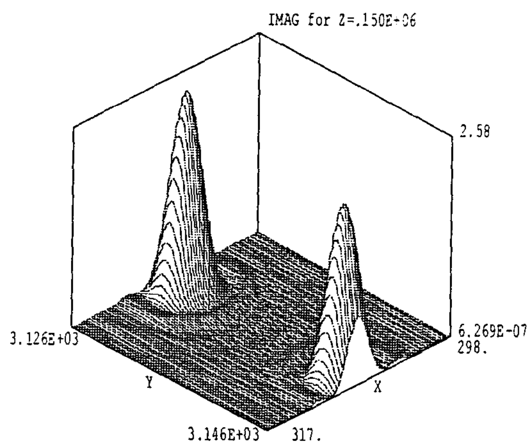

4. CONCLUSION

Stray light analysis has been carried out for the main laser section of the National Ignition facility using a comprehensive non-sequential ray trace model and other tools. The optical configuration has been shown to be free of potentially damaging ghost foci near optical surfaces. Stray light fluences have been calculated for surfaces of mechanical structures; non-metallic absorbers will be located where needed near optical surfaces to avoid the deposition of metal ablation products onto the optics. Baffles will be used to limit grazing incidence reflections from beam tubes. High energy, cavity-type beam dumps will be used to absorb stray light passes in the multipass amplifier. Two spatial filter lenses are tilted to shorten ghost stay-out zones and deflect high energy ghost beams into baffles. Pencil beams that propagate through the system have been modeled and found to not cause potentially damaging fluences at optical surfaces.

Stray light control requirements are being documented by ghost stay-out zones shown on optical configuration drawings, ghost catalogs, material specifications, and drawings for baffles and absorbers.

5. ACKNOWLEDGEMENTS

Work performed under the auspices of the U.S. Department of Energy by Lawrence Livermore National Laboratory under contract W-7405-Eng-48.

6. REFERENCES

1. For additional description of the main laser system see: J. L. Miller, R. E. English, R. J. Korniski, and M. R. Rodgers, "Optical design of the National Ignition Facility main laser and switchyard/target area beam transport systems," in these conference proceedings.